Micro-mechanical modelling of high cycle fatigue behaviour of metals under multiaxial loads

C. Robert [a,b,*], N. Saintier [b], T. Palin-Luc [b], F. Morel [a]

[a] Arts et Metiers ParisTech, LAMPA, 2 bd du Ronceray, 49035 Angers Cedex, France
[b] Arts et Metiers ParisTech, I2M – CNRS, Université Bordeaux 1, Esplanade des Arts et Métiers, 33405 Talence Cedex, France

Keywords:
Multiaxial high cycle fatigue
Finite element simulation
Polycrystalline aggregates
Cubic elasticity
Crystal plasticity

A B S T R A C T

An analysis of high cycle multiaxial fatigue behaviour is conducted through the numerical simulation of polycrystalline aggregates using the finite element method. The metallic material chosen for investigation is pure copper, which has a Face Centred Cubic (FCC) crystalline microstructure. The elementary volumes are modelled in 2D using an hypothesis of generalised plane strain and consist of 300 equi-probability, randomly oriented grains with equiaxed geometry. The aggregates are loaded at levels equivalent to the average macroscopic fatigue strength at 10^7 cycles. The goal is to compute the mechanical quantities at the mesoscopic scale (i.e., average within the grain) after stabilization of the local cyclic behaviour. The results show that the mesoscopic mechanical variables are characterised by high dispersion. A statistical analysis of the response of the aggregates is undertaken for different loading modes: fully reversed tensile loads, torsion and combined in-phase tension–torsion. Via the calculation of the local mechanical quantities for a sufficiently large number of different microstructures, a critical analysis of certain multiaxial endurance criteria (Crossland, Dang Van and Matake) is conducted. In terms of material behaviour models, it is shown that elastic anisotropy strongly affects the scatter of the mechanical parameters used in the different criteria and that its role is predominant compared to that of crystal plasticity. The analysis of multiaxial endurance criteria at both the macroscopic and mesoscopic scales clearly show that the critical plane type criteria (Dang Van and Matake) give an adequate estimation of the shear stress but badly reflect the scatter of the normal stress or the hydrostatic stress.

1. Introduction

The numerical simulation of polycrystalline metal aggregates has seen increased used over the last twenty years (Meric and Cailletaud, 1991) to shed new light on the relationships between the mechanical properties of polycrystalline materials at the scale of individual grains and the overall response of the material within a Representative Elementary Volume (REV). Although much of this work has been focused on the monotonic mechanical behaviour, studies dedicated to fatigue behaviour are becoming more frequent. Bennett and McDowell (2003) have used several mechanical quantities (the maximum slip amplitude, an equivalent stress inspired by the Dang Van criterion (Dang Van, 1973) and an equivalent strain inspired by the Fatemi and Socie criterion (Fatemi and Socie, 1988)) computed at the scale of the grains in order to treat the problem of high cycle fatigue crack initiation. The distributions of these mechanical quantities in polycrystalline aggregates were analysed for two loading modes (tension/compression and shear) with or without mean stress and at different load levels. To test the ability of these

* Corresponding author at: Arts et Metiers ParisTech, LAMPA, 2 bd du Ronceray, 49035 Angers Cedex, France. Tel.: +33 2 41 20 73 27; fax: +33 2 41 20 73 20.
E-mail addresses: camille.robert@ensam.eu (C. Robert), nicolas.saintier@ensam.eu (N. Saintier).

Nomenclature

$\boldsymbol{\Sigma}$	macroscopic stress tensor	τ_r	resolved shear stress (see Fig. 1)
$\boldsymbol{\sigma}$	mesoscopic stress tensor	$\underline{\tau}$	shear stress vector (see Fig. 1)
$\underline{n}$	unit vector normal to the slip plane (see Fig. 1)	τ_{oct}	octahedral shear stress
$\underline{l}$	unit vector in the slip direction (see Fig. 1)	σ_n	normal stress
$\boldsymbol{m}$	orientation tensor for a slip system		

quantities to reflect certain experimental observations, the authors establish a correlation between the distributions of the initiation parameters obtained for alternating tensile loads and distribution of crack lengths observed on the surface of a ferrito-martensitic steel subjected to the same loading type. The results are promising for the Fatemi and Socie type parameter and for the parameter based on the maximum slip amplitude.

Guilhem et al. (2010) continued the work of Bennett and McDowell (2003) and enriched the crack initiation analysis by taking into account the effects of a free surface and the anisotropic elastic material behaviour. The distributions of the various parameters were studied, distinguishing the position of the grains (i.e., in the thickness or on the surface), their direction and the orientation of neighbouring grains. The authors find that the Dang Van equivalent stress and the Fatemi and Socie equivalent slip amplitude do not highlight the well know critical character of the grains at the free surface when considering high cycle fatigue behaviour.

Bertolino et al. (2007) use the concept proposed by Dang Van, whereby elastic shakedown of the grains can be seen as a limit for crack initiation. They therefore sought to determine, using numerical models, the critical load above which at least one grain does not elastically shakedown. This seems to give good predictions for alternating uniaxial tensile loads but not for shear loads. Indeed, in this case, the predicted fatigue limit is under estimated.

Przybyla and McDowell (2010) have studied the interaction effects between different microstructures for the extreme values of the Fatemi and Socie criteria. Several stress levels are studied for uniaxial loads. The authors analysed these distributions for 25–100 Statistical Volume Elements (SVE). They show that these distributions are well characterised by a Gumble type distribution, and converge with this distribution, even for a small number of SVE (i.e., 25).

Parallel to the development of these approaches, recent work by Altus (2006), Morel and Huyen (2008) and Poncelet et al. (2010) have made it possible to take into account the role of microstructural heterogeneities in terms of multiaxial fatigue modelling. These models seek to account for the effect of the variability of the mechanical behaviour at the scale of the microstructure, as simply as possible. For metallic materials, the fatigue crack initiation mechanisms in the HCF regime result in isolated microcracks with no interaction between neighbouring initiated cracks (Flaceliere et al., 2007). Moreover, when an isolated microcrack is not stopped by a microstructural barrier, it may lead to the final failure. To reflect this behaviour from a probabilistic point of view, the weakest link hypothesis (Weibull, 1939, 1951) is often used when it comes to deal with high cycle fatigue. Furthermore, Monchiet et al. (2006, 2008) propose to extend the framework of crystal plasticity by computing damage at the grain scale. The proposed criterion seems to be promising, especially for high hydrostatic pressure.

This study is undertaken in the context of understanding the role of microstructural heterogeneities on the multiaxial high cycle fatigue response via the numerical simulation of polycrystalline aggregates. In this work, the material investigated is pure copper.

The principal components of this work are:

- To investigate the role of the material behaviour (i.e., cubic elasticity and crystal plasticity) and the grain orientation on the mechanical response under cyclic loads at levels close to the average macroscopic fatigue limit at 10^7 cycles.

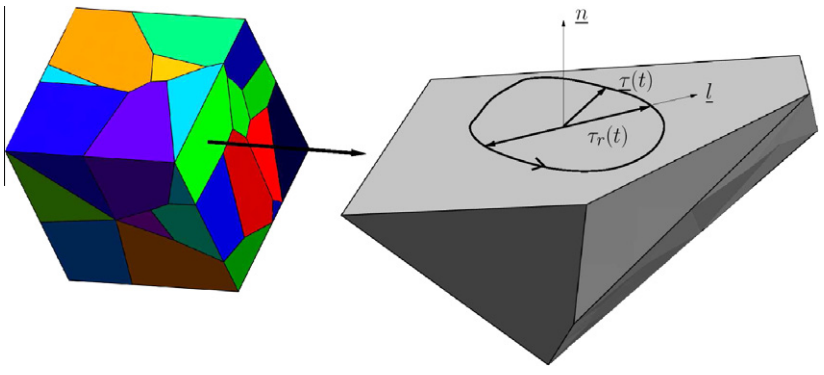

Fig. 1. The definition of certain quantities at the mesoscopic scale.

- To undertake an analysis of the distribution of the mesoscopic mechanical parameters (i.e., the shear stress on a slip plane, the resolved shear stress in a slip system, the hydrostatic stress and the stress normal to a slip plane) for different aggregates and for different macroscopic, fully reversed cyclic loads (i.e., tension, shear and combined in phase tension–shear).
- To investigate the ability of the Crossland, Dang Van and Matake multiaxial fatigue criteria to reflect certain trends observed in HCF under multiaxial loading conditions through the results of the numerical simulations. Particular attention is given to the difference between the macroscopic predictions and the mesoscopic results of the aggregates for each criterion.

2. Numerical procedure

This section discusses the different aspects of the modelling approach. After describing the different material behaviour models used, the finite element models are presented.

2.1. Material behaviour models

In this work, four types of material behaviour, all associated with copper, are studied:

- isotropic elasticity;
- cubic elasticity;
- isotropic elasticity + crystal plasticity;
- cubic elasticity + crystal plasticity.

For the case of isotropic elasticity, the elastic properties of the material are identical in all directions and are characterised by Young's modulus and Poisson's ratio. Furthermore, all grains are assumed to have the same properties. The cubic elasticity material constitutive law is characterised by 3 independent elastic constants. The elasticity coefficients are the same for all grains (in their respective coordinate systems), and each grain has a different orientation, defined by three Euler angles. Crystal plasticity is considered in the classical manner, in which plastic slip occurs in a slip system defined by a plane and a direction in the planes of maximum atomic density. The crystal plasticity law includes combined non-linear isotropic and kinematic hardening. Each grain has 12 slip systems (i.e., an FCC crystal structure) and all of the grains have a different orientation. This plasticity model is described in details in the following section.

One of the objectives of this work is to better understand the effect of the choice of the material constitutive law on the local distributions of the aforementioned mechanical quantities. For this, the effect of cubic elasticity and crystal plasticity on the response at the mesoscopic scale (i.e., the scale of individual grain) are discussed.

For the case of isotropic elasticity, Young's modulus is 50 GPa and Poisson's ratio of 0.3 ($C_{11} = 67.3$ MPa, $C_{12} = 28.8$ MPa and $C_{44} = 38.5$ MPa in Voigt notation). For cubic elasticity, the following constants are used: $C_{11} = 159$ MPa, $C_{12} = 121.9$ MPa and $C_{44} = 80.9$ MPa (Meric and Cailletaud, 1991).

The crystal plasticity material constitutive law used in this work was introduced by Meric and Cailletaud (1991). It is commonly used for the numerical simulation of polycrystalline aggregates (Musienko et al., 2007; Barbe and Quey, 2011; Aubert et al., 2012).

The constitutive relations are defined by Eqs. (1)–(6), where γ^s represents the plastic slip within system s and v^s is the accumulated plastic slip in system s. The isotropic hardening is defined in each slip system by the variable r^s, and the kinematic hardening by the variable x^s. c and d are parameters of the constitutive law.

The orientation tensor $\boldsymbol{m}^s$, which is computed for each slip system s by the tensorial product of the normal to the slip plane $\underline{n}^s$ and the direction of slip $\underline{l}^s$, is used to compute the resolved shear stress τ^s and the plastic strain rate tensor, $\dot{\boldsymbol{\varepsilon}}^{pl}$. The two material parameters, K and n, represent the sensitivity to strain rate. Finally, the parameters r_0, Q and b (and also the components h_{rs} of the interaction matrix) are used to model the isotropic hardening.

The material parameters used for the crystal plasticity, identified for a high-purity copper by Gérard et al. (2009), are presented in Table 1.

$$\dot{\gamma}^s = \left\langle \frac{\|\tau^s - x^s\| - r^s}{K} \right\rangle^n \operatorname{sign}(\tau^s) = \dot{v}^s \operatorname{sign}(\tau^s) \tag{1}$$

$$x^s = c\alpha^s \quad \text{with } \dot{\alpha}^s = \dot{\gamma}^s - d\dot{v}^s\alpha^s \tag{2}$$

$$r^s = r_0 + Q\sum_r h^{rs}(1 - \exp(-bv^r)) \tag{3}$$

$$\boldsymbol{m}^s = (\underline{n}^s \otimes \underline{l}^s + \underline{l}^s \otimes \underline{n}^s)/2 \tag{4}$$

$$\tau^s = \boldsymbol{m}^s : \boldsymbol{\sigma} \tag{5}$$

$$\dot{\boldsymbol{\varepsilon}}^{pl} = \sum_s \dot{\gamma}^s \boldsymbol{m}^s \tag{6}$$

2.2. Loading conditions

The polycrystalline aggregates considered in this work are subjected to load levels corresponding to the average macroscopic fatigue limit at 10^7 cycles, taken from the results of Lukás and Kunz (1989). The fully reversed tensile and torsional fatigue limit used are $s_{-1} = 56$ MPa and $t_{-1} = 36$ MPa respectively. From these data the Crossland criterion, which is defined below, is arbitrarily used to define the equivalent multiaxial loading conditions in tension, shear and combined in-phase tension–shear for all analyses regardless of the criterion being investigated.

For all load conditions investigated, the load ratio used is $R_\sigma = \sigma_{\min}/\sigma_{\max} = -1$ and in the case of combined tension–shear, the biaxiality ratio is $\sigma_a/\tau_a = 1$. These fatigue limits are presented in Table 2.

2.3. The numerical model

The generation of synthetic polycrystalline microstructures has been the subject of numerous studies (Groeber et al., 2008; St-Pierre et al., 2008; Bhandari et al., 2007; Fritzen et al., 2009). Among the most widely used methods,

Table 1
Material parameters used in this work, taken from Gérard et al. (2009).

K (MPa $s^{\frac{1}{n}}$)	n (–)	r_0 (MPa)	Q (MPa)	b (–)	c (MPa)	d (–)	h_0 (–)	h_1 (–)	h_2 (–)	h_3 (–)	h_4 (–)	h_5 (–)
8	20	15	4	12	32,000	900	1	1	0.2	90	3	2.5

Table 2
Tensile and shear stress amplitudes used for the different loading conditions.

	Tension	Shear	Tension/shear
σ_a (MPa)	56	0	30
τ_a (MPa)	0	36	30

the simplest is to create grains of the same topology and to duplicate them in order to fill the entire volume of the microstructure. This relatively simple method allows for the rapid generation of numerical microstructures, even though they may have significant topological differences with real microstructures. This method is used for example by Bridier et al. (2009) with a hexagonal grains topology. Many authors (e.g., Weyer et al. (2002); Zhang et al. (2005); Luther and Könke (2009)) use Voronoi polyhedra to generate more realistic Microstructures. Groeber et al. (2008) have used several Voronoi polyhedra to define the geometry of a grain. This results in a more realistic geometry. Finally, even more sophisticated methods can be used as per St-Pierre et al. (2008) or Bhandari et al. (2007) in order to model curved boundaries and to obtain more representative microstructures.

In order to numerically generate polycrystalline aggregate morphologies, the grains are initially approximated by ellipses (with a randomly chosen minor to major axis ratio of between 0.9 and 1). The ellipses are randomly positioned and orientated but not superimposed. The Watershed algorithm (Fernand and Meyer, 1994) is then used to dilate the ellipses in order to fill the elementary volume. Finally, a CAD model is created by approximating the grain boundary with Bezier curves, and a finite element mesh is generated using Gmsh (Geuzaine and Remacle, 2009). All of these steps are shown in Fig. 2.

For all of the loading conditions studied here, three microstructural topologies containing 300 equiaxed grains were used. In addition, for each topology three sets of random grain orientations are studied. This results in a total of nine configurations. The size of the 2D aggregate is 0.5 mm × 0.5 mm.

For the nine configurations studied, 10 loading cycles were applied. The decision to simulate only 10 cycles is discussed in Section 4. The microstructures and the finite element mesh are periodic with respect to the two axes. The different topologies and different orientations are shown in Fig. 3. The different grain orientations are presented in the form of pole figures.

Triangular (3 node) finite elements, with linear interpolation, are used with an hypothesis of generalised plane strain. Each grain contains approximately 400 linear elements. An example of a meshed microstructure is shown in Fig. 4.

The boundary conditions consist of an imposed mean stress (i.e., imposed on the entire aggregate), with periodic displacement conditions at the edges of the aggregate.

The ZeBuLoN finite element code is used. This software is developed by Mines ParisTech, Northwest Numerics and ONERA.

3. Multiaxial endurance criteria

3.1. Crossland criterion

The Crossland criterion (Crossland, 1956) is based on a macroscopic approach. It takes into account two mechanical quantities, the magnitude of the octahedral shear stress $\tau_{\mathrm{oct},a}$ and the maximum hydrostatic stress $\sigma_{\mathrm{hyd,max}}$. It is formulated as follows:

$$\tau_{\mathrm{oct},a} + \alpha_c \sigma_{\mathrm{hyd,max}} \leqslant \beta_c \tag{7}$$

where $\alpha_c = \frac{t_{-1} - s_{-1}/\sqrt{3}}{s_{-1}/3}$ and $\beta_c = t_{-1}$ are the criterion coefficients and can be identified from the fully reversed tensile and torsional fatigue limits (s_{-1} and t_{-1}).

The amplitude of the octahedral shear stress is defined by:

$$\tau_{\mathrm{oct},a} = \sqrt{J_{2,\mathrm{amp}}(\boldsymbol{\sigma})} \tag{8}$$

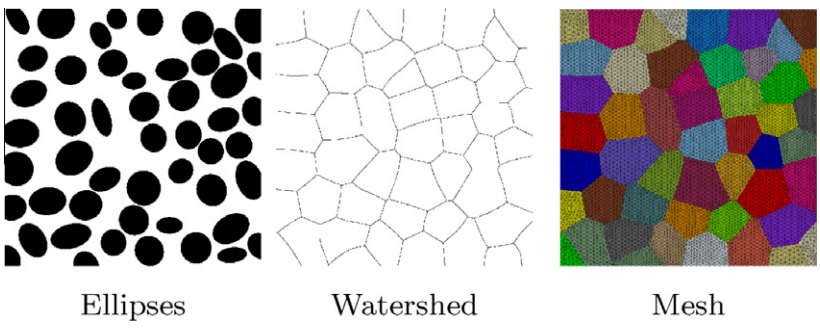

Fig. 2. The principal steps used to generate the mesh of the finite element models of the polycrystalline aggregates.

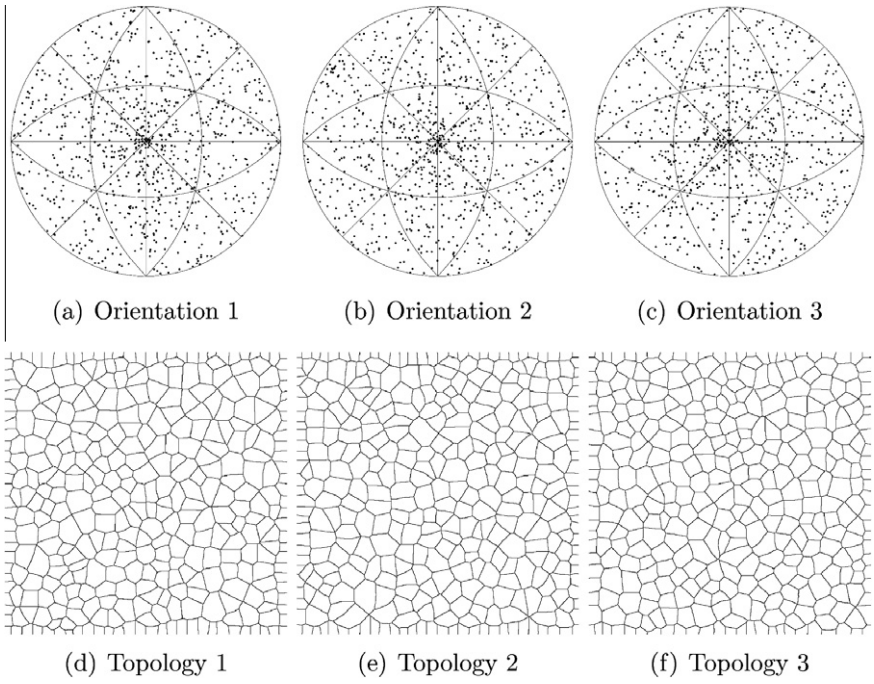

Fig. 3. (a)–(c) Pole figures (100) showing the three different grain orientations and (d)–(f) the three different topologies investigated.

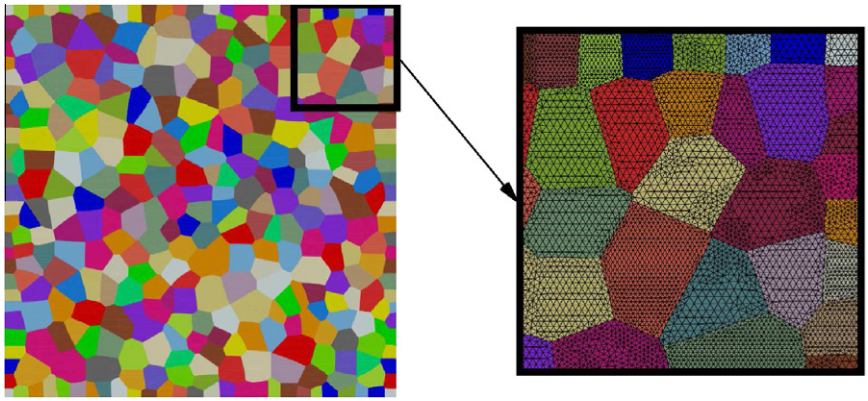

Fig. 4. The finite element mesh of a periodic aggregate with 300 grains and approximately 120,000 elements.

where $J_{2,\mathrm{amp}}(\boldsymbol{\sigma})$ is determined from the smallest hypersphere circumscribing the loading path in the deviatoric space associated with the tensor $\boldsymbol{\sigma}$. More precisely $J_{2,\mathrm{amp}}(\boldsymbol{\sigma})$ is the radius of this hypersphere when the norm J_2 is used. J_2 is the second invariant of deviatoric stress:

$$J_2 = \frac{1}{2} S_{ij} S_{ij} \tag{9}$$

and $\boldsymbol{S}$ is the deviatoric stress tensor defined by:

$$\boldsymbol{S} = \boldsymbol{\sigma} - \frac{1}{3} tr(\boldsymbol{\sigma}) \mathbf{I} \tag{10}$$

$\boldsymbol{I}$ is the second order unit tensor.

3.2. Dang Van criterion

The Dang Van multiaxial criterion (Dang Van, 1973) is valid in the high cycle fatigue domain and is a multi-scale approach based on the concept of elastic shakedown.

The Lin–Taylor hypothesis (Taylor, 1938; Lin, 1957) is used for the scale transition from mesoscopic to macroscopic quantities. The criterion can be summarised by the following statement: "Microscopic fatigue crack initiation does not occur if the material achieves an elastic shakedown state at both the macroscopic and mesoscopic scales". Mathematically the criterion is represented by Eq. (11)

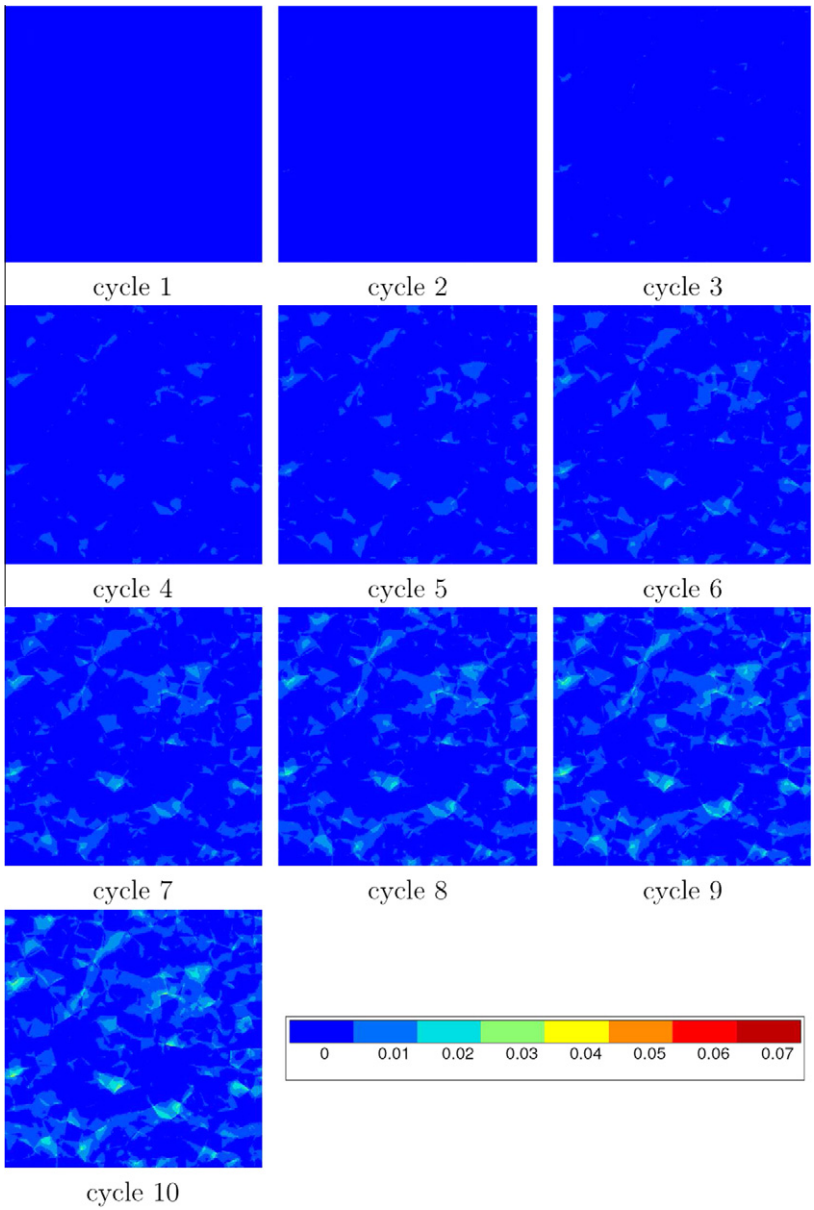

Fig. 5. Evolution of the accumulated equivalent plastic strain at the end of each cycle for the tensile loading condition using the cubic elasticity + crystal plasticity material constitutive law.

$$\max_{t}\left\{\max_{\underline{n}}\left[\left\|\underline{\widehat{\tau}}(\underline{n},t)\right\|+\alpha_{dv}\,\widehat{\sigma}_{\mathrm{hyd}}(t)\right]\right\}\leqslant\beta_{dv} \tag{11}$$

where $\widehat{\sigma}_{\mathrm{hyd}}(t)$ and $\widehat{\boldsymbol{\sigma}}(t)$ are time functions of the hydrostatic stress and the stress tensor after elastic shakedown given by:

$$\widehat{\sigma}_{\mathrm{hyd}}(t)=\frac{1}{3}\widehat{\sigma}_{ij}(t) \tag{12}$$

and $\underline{\widehat{\tau}}(\underline{n},t)$ is the mesoscopic shear stress after shakedown on a plane defined by its normal vector, $\underline{n}$.

$\alpha_{dv}=\frac{t_{-1}-s_{-1}/2}{s_{-1}/3}$ and $\beta_{dv}=t_{-1}$ are two criterion coefficients that can be identified from the fully reversed tensile and torsional fatigue limits (s_{-1} and t_{-1}).

3.3. Matake criterion

The Matake criterion (Matake, 1977) is based on a critical plane approach. It takes into account two mechanical quantities: the shear stress amplitude τ_a and the maximum normal stress $\sigma_{n,\max}$. The criterion is formulated as follows:

$$\max_{\underline{n}}(\tau_a)+\alpha_m\sigma_{n^*,\max}\leqslant\beta_m \tag{13}$$

where n^* is the normal to the slip plane for which the shear stress amplitude (τ_a) is maximum. The two criterion coefficients, $\alpha_m=2\frac{t_{-1}}{s_{-1}}-1$ and $\beta_m=t_{-1}$ can be identified from

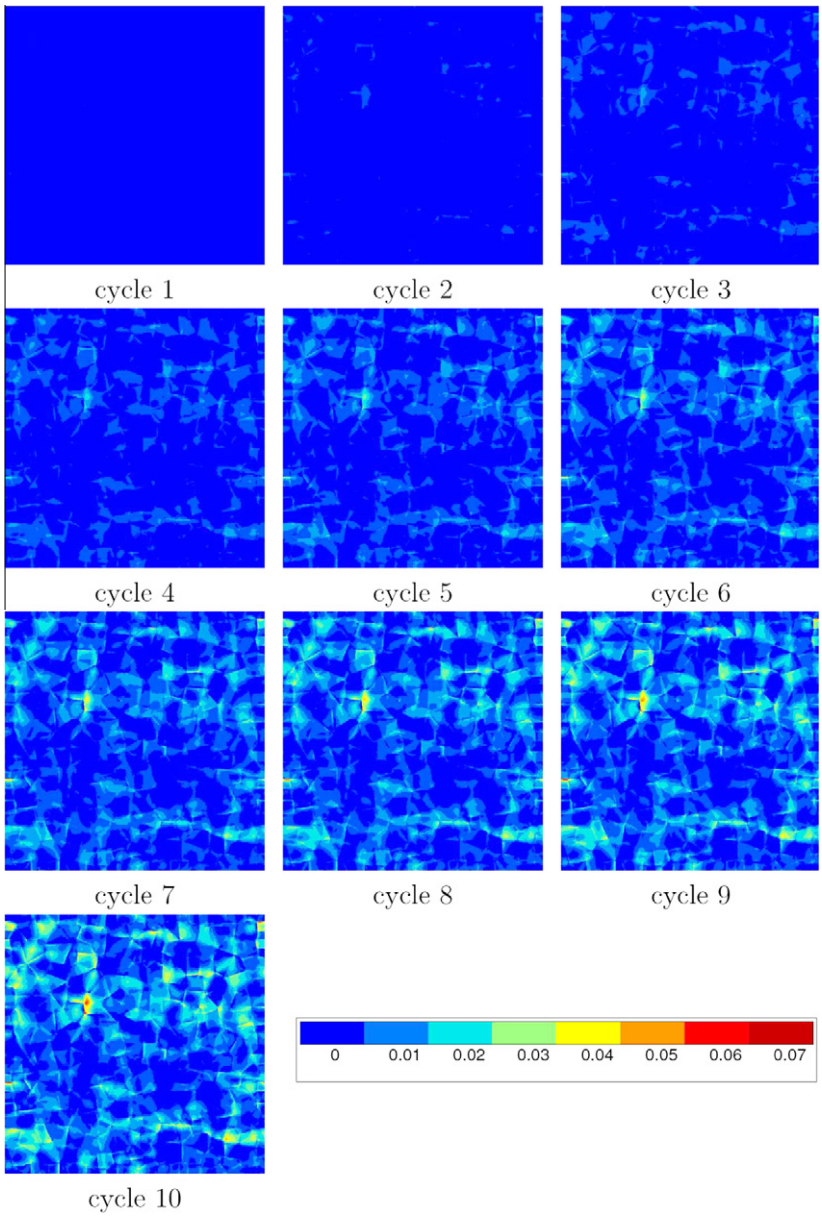

Fig. 6. Evolution of the accumulated equivalent plastic strain at the end of each cycle for the fully reversed shear loading condition using the cubic elasticity + crystal plasticity material constitutive law.

the fully reversed tensile and torsional fatigue limits (s_{-1} and t_{-1}).

4. Results

This section presents the cyclic response for the different material behaviour models and the three loading modes. Firstly, Figs. 5–7 highlight the spatial evolution of the accumulated equivalent plastic strain (γ^{cum}), during the first 10 cycles, for the cubic elasticity + crystal plasticity material constitutive law, and for the three loading modes studied. Note that these values are not values averaged in the grains but are the values at each integration point of the FE mesh. It can be seen that the most plastified grains, in terms of accumulated equivalent plastic strain, during the first cycles remains the most plastified throughout the following cycles. Moreover, a strong variation of this quantity (or large heterogeneity) is observed between the different grains. Regarding the influence of the loading type, the intensity of the accumulated equivalent plastic strain after cycling is greater for shear loading (Fig. 6) compared to the tensile load case (Fig. 5). Also, for the shear load case there are more grains for which this quantity is high. As for the combined tension–shear load case (Fig. 7) the intensity of the maximum accumulated plastic deformation is in between the tensile and shear cases. In shear

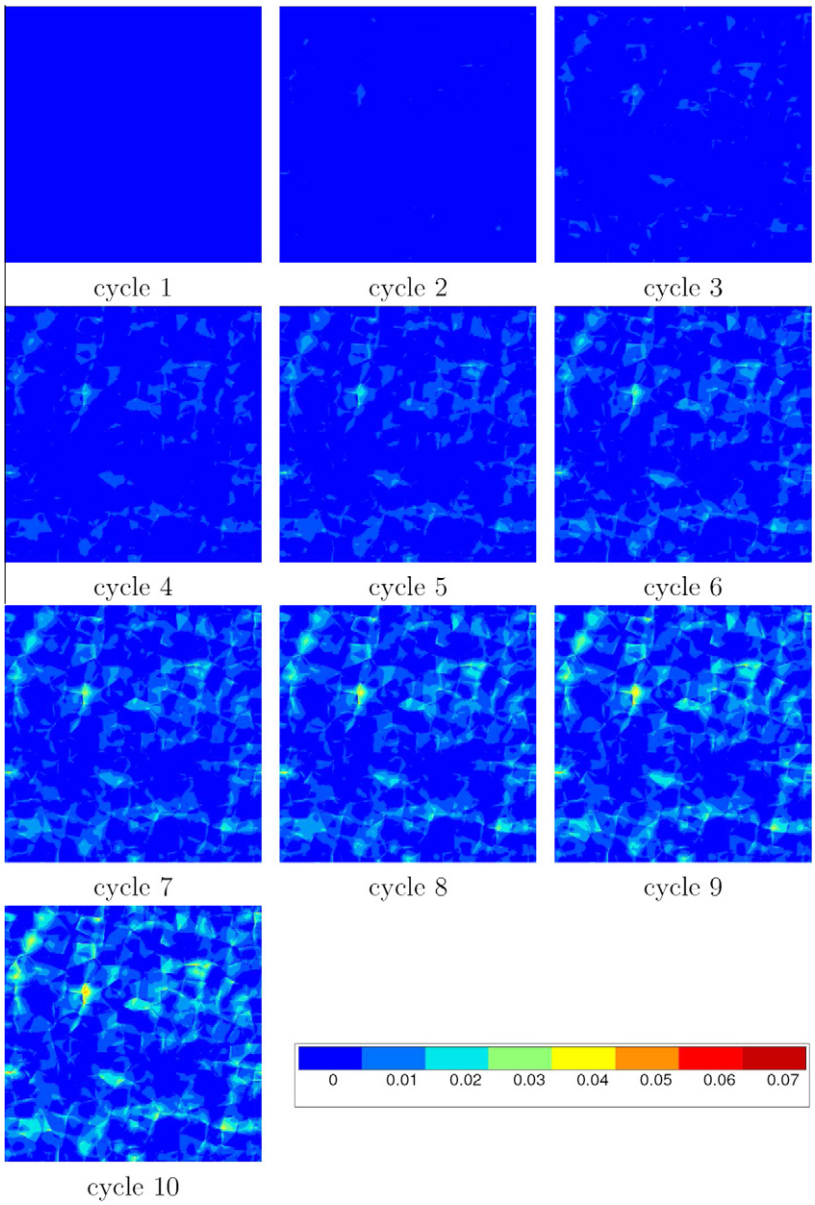

Fig. 7. Evolution of the accumulated equivalent plastic strain at the end of each cycle for the tension/shear loading condition using the cubic elasticity + crystal plasticity material constitutive law.

17% of grains have $\gamma^{\text{cum}} > 0.5\gamma^{\text{cum}}_{\text{max}}$ compared to the tensile loading case for which 10% of grains have $\gamma^{\text{cum}} > 0.5\gamma^{\text{cum}}_{\text{max}}$ and for the tension/shear loading case 15% of grains have $\gamma^{\text{cum}} > 0.5\gamma^{\text{cum}}_{\text{max}}$. This is also experimentally observed (Agbessi et al., 2011). The maximum mesoscopic (or grain averaged value) of γ^{cum} is 0.032 for the shear loading case, 0.021 for the tensile loading case and 0.026 for tension/shear. Also in tension/shear the grains for which the plasticity is well developed are identical to the shear load case.

4.1. Mechanical response of the polycrystalline aggregates

The results are presented for both the mesoscopic and the macroscopic scale.

The macroscopic scale represents the average behaviour of the complete aggregate. The mechanical quantities are computed from the stress tensor, associated with the imposed load. The macroscopic stress is referred to as $\boldsymbol{\Sigma}$.

The mesoscopic scale represents the behaviour in a grain. The mechanical quantities are the volumetric average in the grain of each component of the stress tensor. Elements having at least one node on the grain boundary are excluded from the averaging process. Hence, stress concentrations at grain boundaries are not taken into account.

Note that, all of the mechanical quantities reported at the mesoscopic scale are averaged quantities within the grains so that the linear interpolation of three nodes ele-

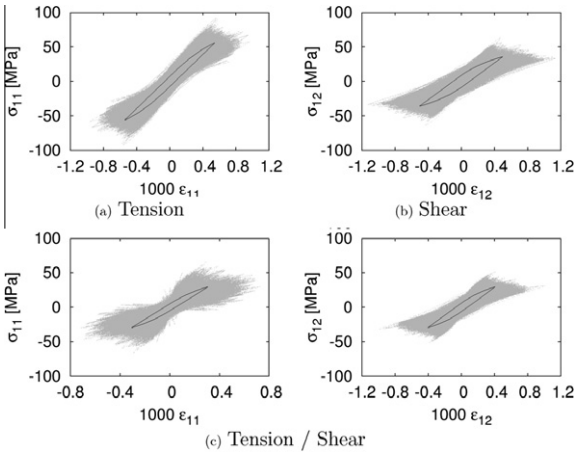

Fig. 8. Cyclic stress–strain behaviour at the macroscopic scale (in black) and the mesoscopic behaviour (in gray) for a simulation using the cubic elasticity + crystal plasticity material constitutive law.

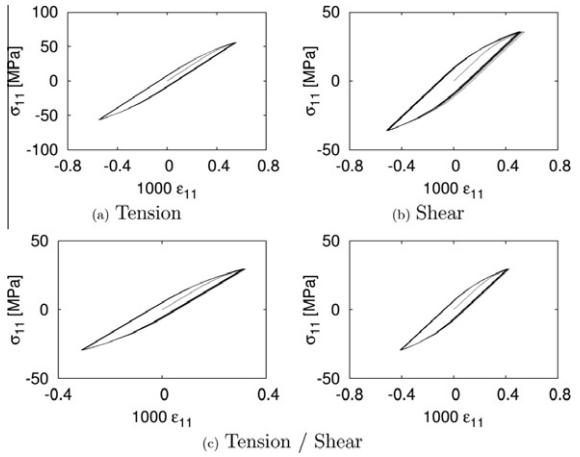

Fig. 9. Cyclic stress–strain behaviour over all cycles at the macroscopic scale for a simulation using the cubic elasticity + crystal plasticity material constitutive law.

ments as a little effect on the average values specially as stress gradient are relatively low.

Fig. 8 shows the stress–strain curves computed at the mesoscopic and macroscopic scales for different loading conditions, for the cubic elasticity + crystal plasticity material constitutive law. The gray zone in these figures correspond to the superposition of the average stress–strain curves for each of the grains. The extent of this gray zone represents the range of values determined at the mesoscopic scale in the elementary volume. The black curve represents the behaviour at the macroscopic scale. It can be seen that there are significant variations in the values of the maximum stress and strain in the grains, which are much higher than the values obtained at the macroscopic scale. Note also that the hysteresis loops are generally centred around zero at the mesoscopic scale.

It can be seen from Fig. 9 that after having applied 10 cycles a stabilized macroscopic stress–strain hysteresis loop is obtained for each loading mode. The CPU time for each simulation is approximately 60 h on an Intel Xeon X5677 processor at 3.47 GHz with 64 Gb of RAM.

4.2. The Crossland criterion

The Crossland diagrams, shown in Fig. 10 are plotted for the three different loading conditions and the four different material constitutive laws. The mechanical quantities are computed for the last cycle. For the mesoscopic scale, the quantities $\tau_{oct,a}$ and $\sigma_{hyd,max}$ are shown for each grain of the nine microstructures studied. At the macroscopic scale these quantities are computed from the stress tensor averaged over the total volume of the aggregate. The criterion prediction at the macroscopic scale is given by the black point which falls on the solid line representing the Crossland macroscopic criterion threshold at 10^7 cycles for a failure probability of 0.5. The cloud of gray dots shows the results at the mesoscopic scale. In these figures, the maximum on the cycle (over time) of the hydrostatic stress for the last cycle is always positive, even for the loading in shear. This implies that no grains are loaded in compression/compression. Fig. 10(a) shows the results for the isotropic elastic material constitutive law. As expected, for the three loading cases, the mesoscopic criterion predictions for each grain are identical to the macroscopic prediction.

4.2.1. The effect of the elasticity model (isotropic and cubic)

Fig. 10(c) and (d) highlights the influence of the elasticity model used in combination with crystal plasticity, on the results of the Crossland criterion. For cubic elasticity, large dispersion of the variables is observed at the mesoscopic scale. For the simulations using isotropic elasticity + crystal plasticity, the difference between the macroscopic and mesoscopic scales is relatively small. This is because in this case where fatigue limits are close to the macroscopic yield limit, the ratio between plastic strain and elastic strain is small.

4.2.2. The effect of crystal plasticity

Fig. 10(b) and (d) highlights the influence of crystal plasticity used in combination with cubic elasticity. In both of these figures, the scatter of the two mechanical variables of this criterion is of the same order of magnitude. Hence, crystal plasticity has less effect than the change from isotropic to cubic elasticity.

For the different load modes studied, the macroscopic result falls within the range of the mesoscopic quantities.

4.3. Dang Van criterion

This criterion at the grain scale is discretized on the different slip systems which correspond to the possible physical planes for crack initiation in a given grain. However at the scale of the aggregate, all the possible planes are considered (as in the continuum space discretization proposed by Dang Van) since the grain orientation distribution considered in this work is uniform, and that sufficient number of grains are considered for each loading type. The angles Θ and Φ (Fig. 14) defining the unit normal vector of the slip

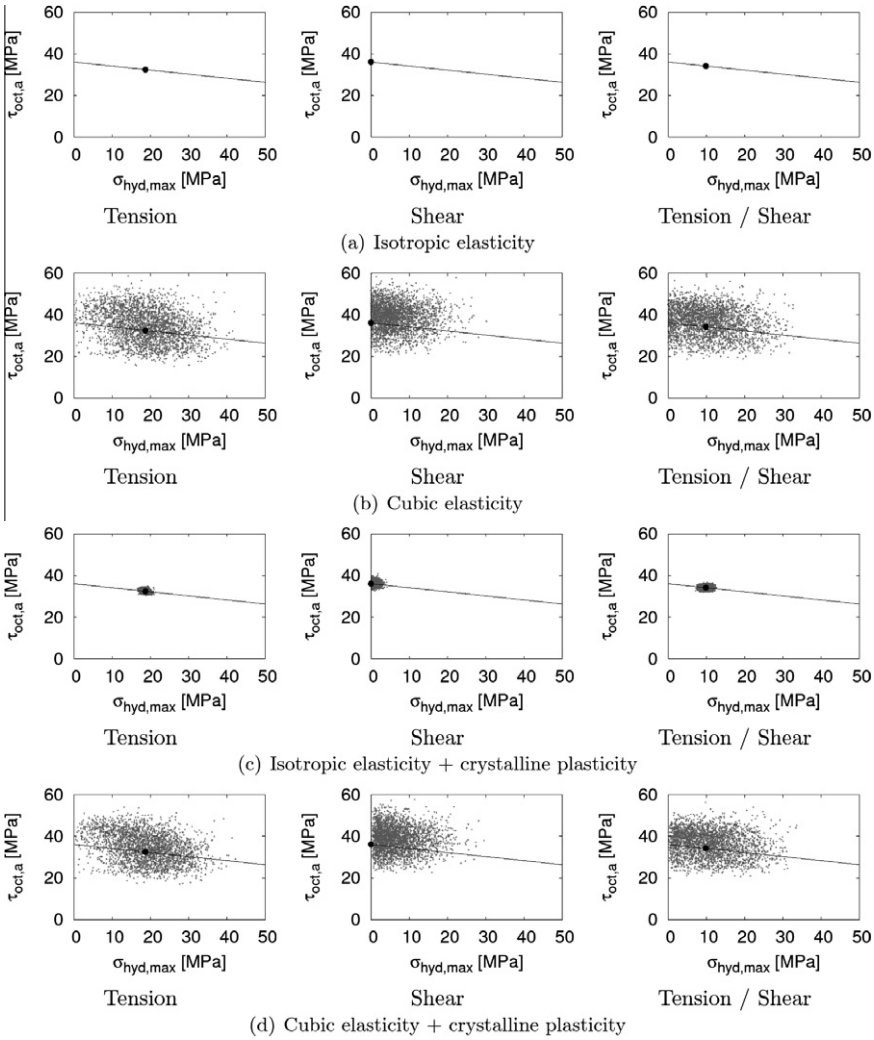

Fig. 10. The prediction from the Crossland criterion at the macroscopic scale (in black) and mesoscopic scale (in gray).

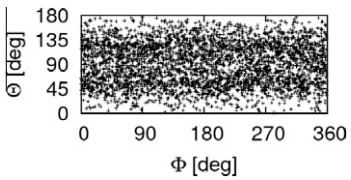

Fig. 11. Illustration of all the considered slip planes within all the aggregate (spherical coordinates of the unit normal vector to the considered planes).

planes are shown in Fig. 11. The norm of shear stress ($\tau(t)$) is used. It can be noted that the ratio $\frac{\tau_m}{\tau_a}$ is small, where τ_m and τ_a are the mean and amplitude of the shear stress, calculated using the smallest circle circumscribing the load path of the tenth load cycle.

The maximum values of $\tau(t) + \alpha_{dv}\sigma_{\text{hyd}}(t)$, as a function of time, determined during the last cycle are computed for each slip plane and the corresponding values of τ, σ_{hyd} are plotted in gray in Fig. 12. The black dot corresponds to the macroscopic value of the criterion by taking into account all possible physical planes. The Dang Van criterion threshold line, computed from the macroscopic fatigue limits, is given by the solid line. Fig. 12(a) shows the results obtained using the isotropic elastic material constitutive law. The hydrostatic stress is identical at both scales. The shear stress on the slip planes, computed at the mesoscopic scale varies from zero to the value obtained at the macroscopic scale. For the combined tension–shear loading mode, the macroscopic point is slightly above the criterion threshold line because the loading conditions are defined from the Crossland criterion.

4.3.1. Comparison with Crossland criterion

In terms of cubic elasticity (Fig. 12(b)) the cloud of gray points representing the mesoscopic results is very dispersed. In addition, some grains have a critical value of this criterion that is beyond the macroscopic endurance threshold. As per the Crossland diagram, the difference between the mechanical quantities used in this criterion, at the

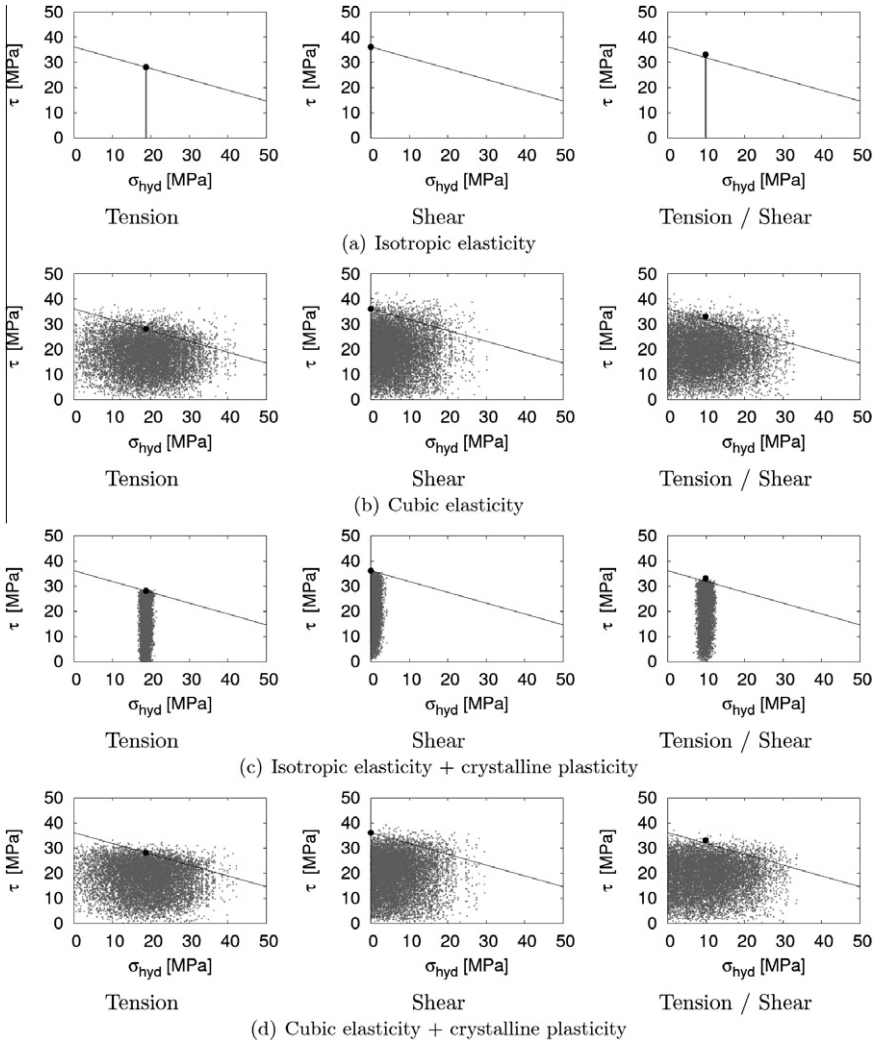

Fig. 12. The predictions from the Dang Van criterion at the macroscopic scale (in black) and the mesoscopic scale (in gray).

two scales, is very significant for the simulations using the cubic elasticity material constitutive law. Also, the maximum shear stress on all slip planes at the mesoscopic scale is greater than the maximum value of macroscopic shear stress for this type of behaviour. Regarding the influence of the crystal plasticity, its role seems limited to a slight increase in the dispersion of the averaged mesoscopic hydrostatic stress for the simulations using isotropic elasticity and a reduction in the maximum shear stress for the case of cubic elasticity (which however remains greater than that computed at the macroscopic scale). In addition, the maximum observed shear stress in the calculations with cubic elasticity is higher than that for the case of isotropic elasticity.

4.3.2. The effect of the material constitutive law on the loading path

Fig. 13 represents the temporal evolution of the two variables used in the Dang Van criterion, at the mesoscopic scale (in gray) and the macroscopic scale (in black). It can be seen that for the isotropic elasticity constitutive law, without crystal plasticity, the maximum values at the mesoscopic scale for each time step are equal to those at the macroscopic scale. For the case of cubic elasticity, the cloud of points representing the mesoscopic scale is very dispersed but globally has the same shape as the macroscopic load path. The crystal plasticity has less impact than cubic elasticity on the overall shape of the mesoscopic loading path.

Note that the black line illustrates the load path on the Dang Van critical plane, while the gray points correspond to all the slip planes of the aggregates.

4.3.3. Critical plane analysis

Fatigue crack initiation is highly dependent on the orientation of slip planes. In a 3D coordinate system the orientation of the normal to the slip planes can be defined using a spherical coordinate system. The normal can be defined by two angles: the angle θ between the z axis and the xy plane of the macroscopic coordinate system and the an-

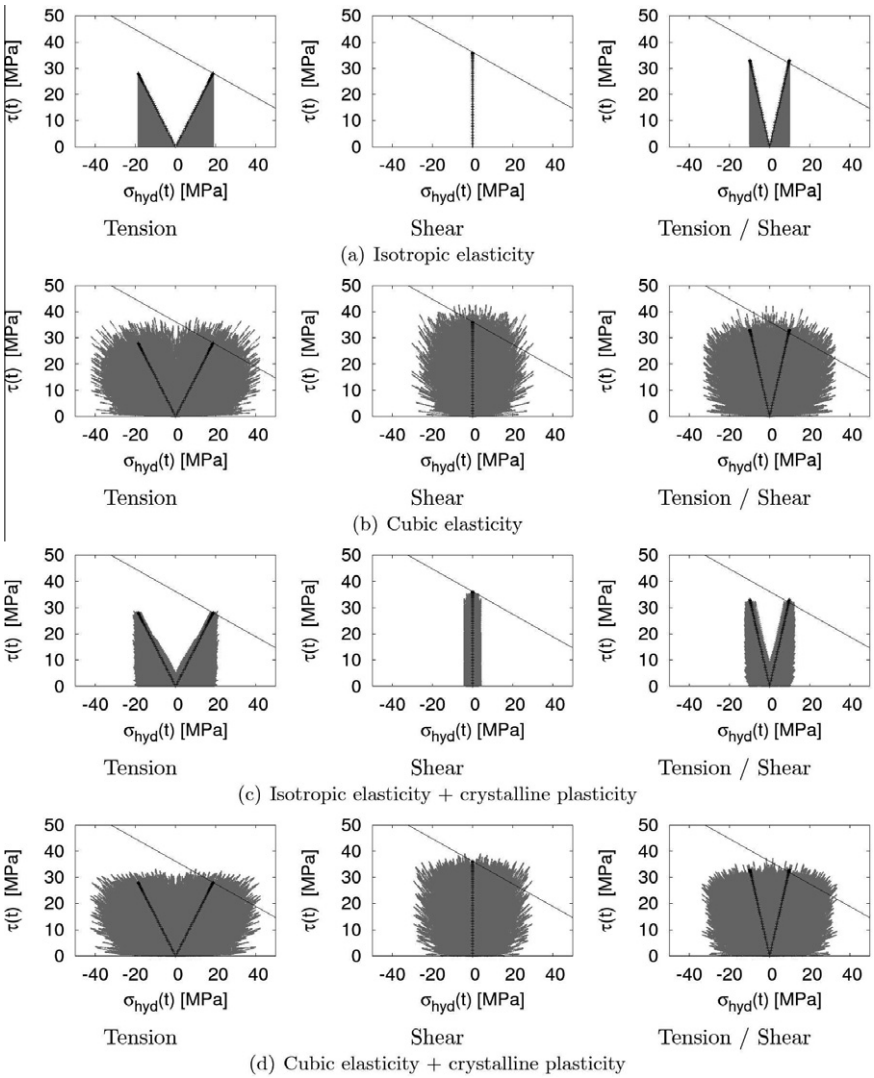

Fig. 13. Temporal evolution of the two variables used in the Dang Van criterion at the macroscopic scale (in black) and the mesoscopic scale (in gray).

gle Φ between the x axes of the macroscopic coordinate system and the plane defined by (n,z) (see Fig. 14).

The coefficient of danger for the Dang Van criterion, for a given slip plane, can be written as follows:

$$D = \max_t \left(\frac{\tau(t) + \alpha \sigma_{\text{hyd}}(t)}{\beta} \right) \tag{14}$$

The coefficient of danger normalised with respect to the microstructure can then be defined by:

$$D_n = \frac{D}{D_{\max}} \tag{15}$$

where $D_{\max}$ is the maximum value of the coefficient of danger for all computed slip planes of the microstructure.

This normalised coefficient of danger is plotted in Fig. 15, in terms of the two angles (θ, Φ), for all simulated slip planes of the polycrystalline aggregates. (Values lower than 0.6 are not plotted.)

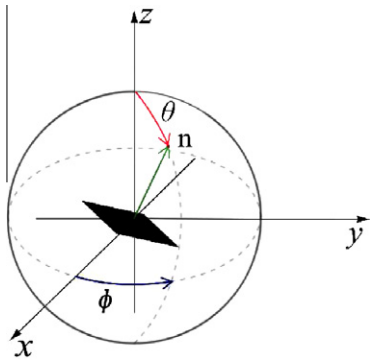

Fig. 14. Spherical coordinate system defining the unit normal vector to a slip plane, where (x,y,z) are linked to macroscopic coordinate system.

In terms of orientation, very little variation of the distribution of the coefficient of danger is seen for the isotropic

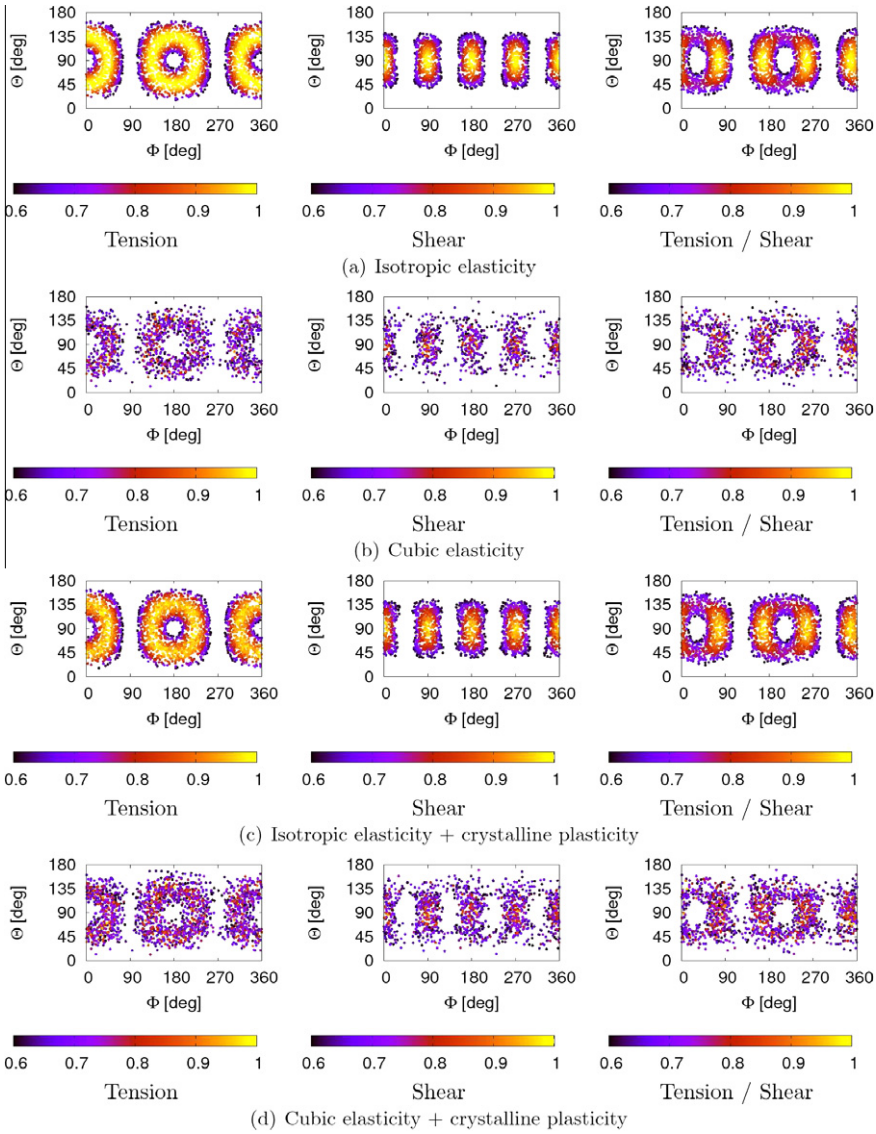

Fig. 15. Normalised coefficient of danger for the Dang Van criterion as a function of the orientation of the normal to the slip plan (values less than 0.6 are not plotted).

elasticity constitutive law, with and without crystal plasticity. For the case of cubic elasticity, some orientations have a coefficient of danger that is much higher than others. Also, the critical plane orientation scatter is much higher compared to the case of isotropic elasticity.

4.4. Matake criterion

Fig. 16 shows the resolved shear stress amplitude as a function of the maximum normal stress determined from the totality of the modelled slip systems. The results of the different loading modes and the different material constitutive laws are shown. As before, the cloud of gray points shows the mesoscopic result for the different slip systems. The black point shows the macroscopic result and the solid line is the Matake criterion threshold line. For the simulations using the isotropic elastic material constitutive law (see Fig. 16(a)), good correspondence is observed between the point representing the macroscopic prediction and the upper part of the envelope of the mesoscopic points, for which the shear stress amplitude is a maximum. This implies that the number of slip system in the aggregate is sufficient to be representative of the number of slip planes in the physical space.

4.4.1. Effect of the material behaviour on the mechanical variables of the criterion

Regarding the influence of the type of material behaviour at the mesoscopic scale, Fig. 16(b) shows that cubic elasticity strongly influences the resolved shear stress amplitude as well as the maximum normal stress. The impact of crystal plasticity combined with isotropic elasticity

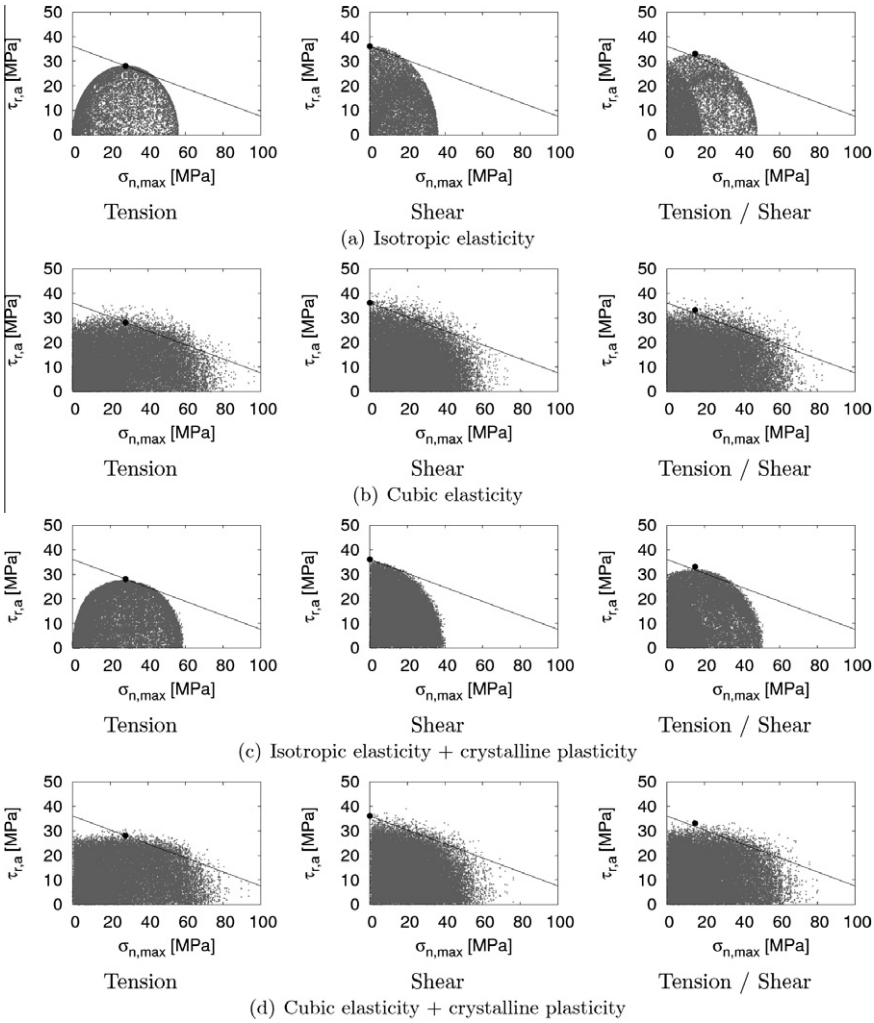

Fig. 16. The predictions from the Matake criterion at the macroscopic scale (in black) and the mesoscopic scale (in gray).

(see Fig. 16(c)) is low when considering the maximum value of the resolved shear stress amplitude. However it increases the maximum normal stress by several percent. In terms of the effect of crystal plasticity combined with cubic elasticity (see Fig. 16(d)), a slight decrease is observed in the maximum resolved shear stress amplitude and maximum normal stress.

5. Discussion

Thanks to the preceding investigation of different high cycle multiaxial fatigue criteria, the dispersion of the mechanical quantities at the mesoscopic scale has been highlighted.

The use of the Crossland criterion, based on a macroscopic approach, shows that the macroscopic point is located roughly in the middle of the cloud of gray points representing the mesoscopic predictions. The use of this criterion therefore results in a macroscopic prediction which corresponds to the "average" mesoscopic behaviour.

From a constitutive point of view at the mesoscopic scale, for the case where the fatigue limit is close to the macroscopic yield stress, crystal plasticity has relatively little effect on the mesoscopic response. However, cubic elasticity (or local anisotropic elasticity) has a considerable influence on the dispersion of the mesoscopic values.

In the case of a local stress approach, the two criteria investigated (i.e., Dang Van and Matake) also highlight the dispersion of the variables computed at the mesoscopic scale. In terms of behaviour, crystal plasticity combined with isotropic elasticity has little effect on the maximum shear stress as well as the amplitude of the maximum resolved shear stress compared to the case of isotropic elasticity, without plasticity. In terms of hydrostatic stress and maximum normal stress, a dispersion of a few percent is observed. However, for these two criteria, the critical values obtained at the mesoscopic scale are very close to those associated with the macroscopic scale. For this type of criteria, cubic elasticity has a strong influence on the results. The maximum shear stress and the amplitude of the

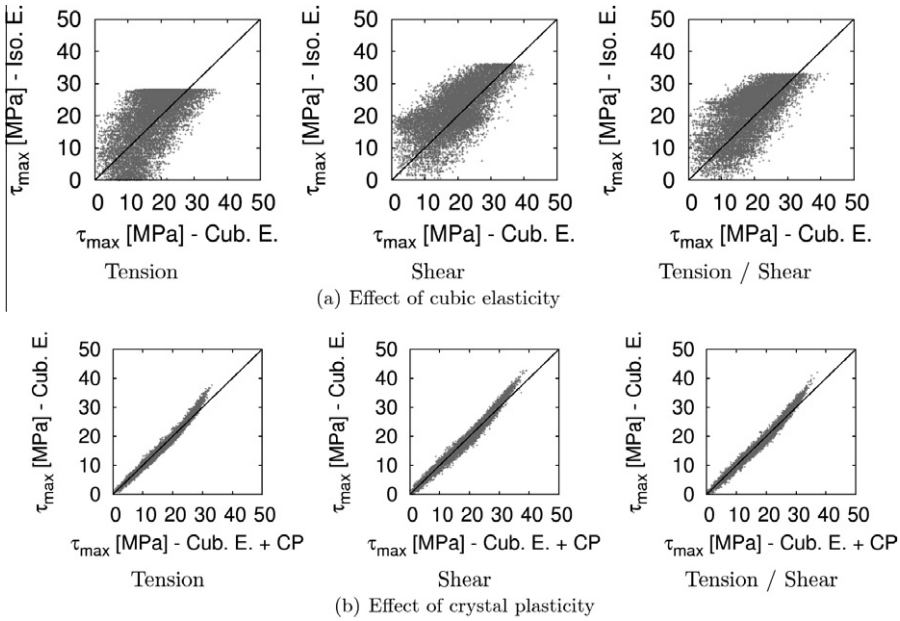

Fig. 17. Comparison of the maximal shear stress (a) between isotropic elasticity (Iso. E.) and cubic elasticity (Cub. E.). and (b) between cubic elasticity (Cub. E.) and cubic elasticity + crystal plasticity (Cub. E. + CP).

maximum resolved shear stress increase significantly with respect to the isotropic elasticity case (even if crystal plasticity tends to decrease them). In terms of the hydrostatic stress, the maximum is more than 20 MPa greater than the maximum value obtained with an isotropic elastic behaviour, for the three studied load cases. Crystal plasticity does not appear to influence these maximum values. For the case of cubic elasticity, it is clear that the mesoscopic hydrostatic stress is not equal to the macroscopic hydrostatic stress, as assumed in the Dang Van criterion.

These differences have a significant impact on the maximum value of the Dang Van coefficient of danger, but in terms of critical planes orientations, the maximums are not strongly modify by cubic elasticity. In terms of the maximum normal stress, its maximum value also increases by the same order of magnitude as the hydrostatic stress.

The maximum shear stress for each slip plane, determined for the last cycle, is plot in Fig. 17(a) for the case of isotropic elasticity and cubic elasticity. The gray points are plotted for the same slip plane. The solid line represents perfect agreement between isotropic elasticity and cubic elasticity. Large dispersion is observed, which is globally centred on the solid line. The largest dispersion is observed for the highest values of the shear stress for the tensile loading condition. This is not the case for the other two loading types.

The maximum shear stress for each slip plane, determined for the last cycle, is plot in Fig. 17(b) for the case of cubic elasticity and cubic elasticity + crystal plasticity. The gray points are plotted for the same slip plane, and the solid line represents perfect agreement between the two behaviour types. It can be seen that crystal plasticity tends to reduce the highest values of the shear stress due to hardening. Lower dispersion is also observed (i.e., "smoothing" effect of the microplasticity).

The maximum resolved shear stress (or the maximum shear stress) increases significantly for a behaviour including cubic elasticity at the mesoscopic scale. To further investigate this particularity, apparent Schmidt factors are analysed in the following. These factors are defined using the following equation:

$$F_S = \max_t \left(\frac{\tau_r(t)}{\Sigma_I(t)} \right) \tag{16}$$

where Σ_I is the largest principal stress at the macroscopic scale.

Fig. 18 shows the accumulated apparent Schmidt factor density, considering all slip systems computed for the nine microstructures, for the different loading modes and for the four material constitutive laws studied. It can be observed that the majority of slip systems have an apparent Schmidt factors with a lower intensity for the cubic elastic case (with or without crystal plasticity). However, for this type of behaviour, the maximum values are much higher. Globally, crystal plasticity tends to reduce the maximum value.

To better understand these curves, the maximum apparent Schmidt factors are plotted as a function of the percentage of the total number of systems (see Fig. 19). The 100th percentile corresponds to all of the simulated slip systems and 90th percentile corresponds to the 90% of systems with the lowest apparent Schmidt factors. For the 90th percentile the tendencies, with respect the type of elasticity, are inverted compared to 100th percentile. The apparent Schmidt factors are lower for cubic elastic behaviour. Crystal plasticity, has a relatively small effect,

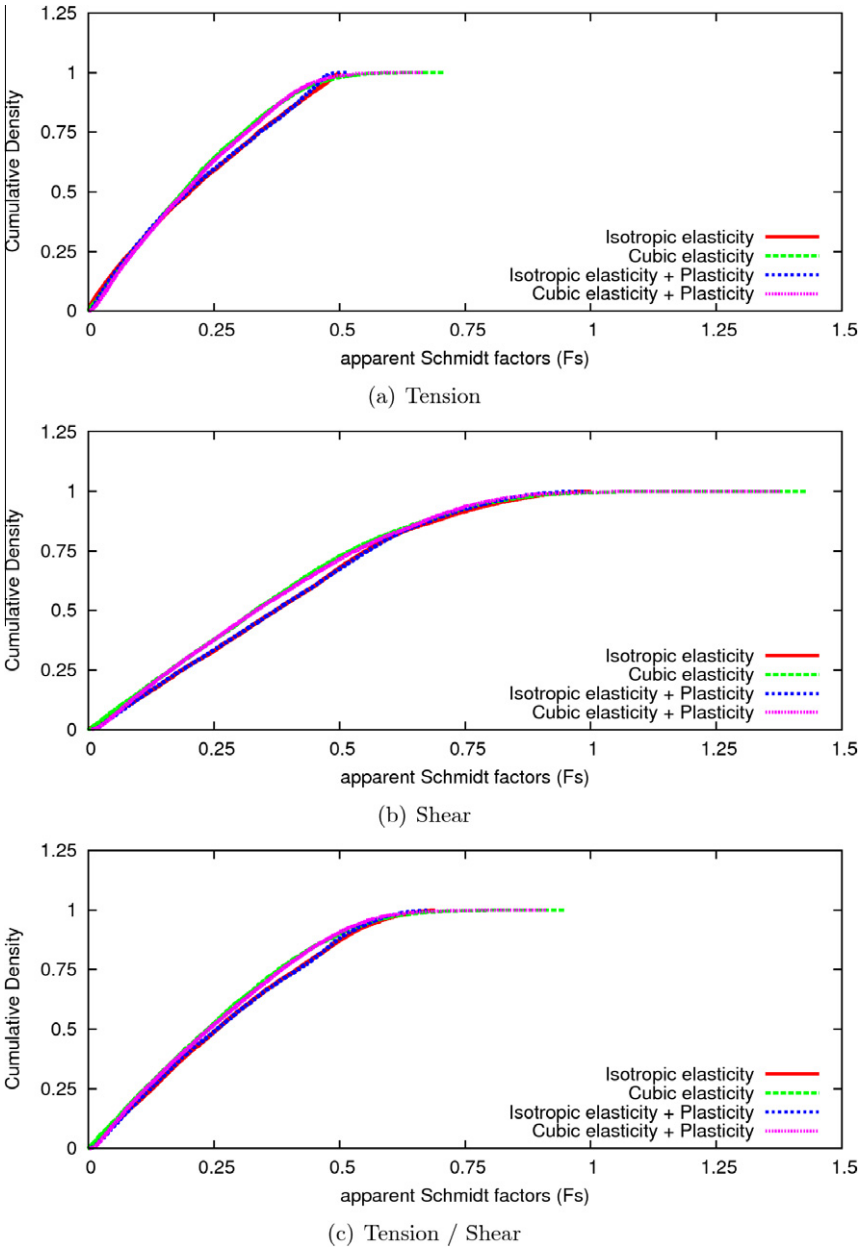

Fig. 18. Density of the apparent accumulated Schmidt factors for the different material constitutive laws studied.

but never-the-less tends to decrease the maximum values, for all the loading modes and the two types of elasticity studied. For the case of uniaxial tension, it goes from 0.44 to 0.43 for isotropic elasticity and from 0.40 to 0.39 for cubic elasticity.

For the case of uniaxial tension Sauzay (2007) studied the effect of the free surface using cubic elasticity on the maximum values of the apparent Schmidt factors. Polycrystalline aggregates with grains modelled using an extruded hexagonal geometry, surrounded by an isotropic homogeneous matrix were considered. He obtained a decrease in the apparent Schmidt factors as a function of the coefficient of anisotropy ($2C_{44}/(C_{11}-C_{12})$). He noted that with a coefficient of anisotropy of 3.26 the maximum apparent Schmidt factor is 0.43. In our work, for the cubic elasticity, without plasticity case (i.e., coefficient of anisotropy equal to 4.36), the maximum apparent Schmidt factor is 0.71 taking into account all grains and becomes equal to 0.40 for the 90th percentile. For the case of isotropic elasticity, these factors are 0.5 and 0.44 respectively. The major difference, with respect to Sauzay's work (Sauzay, 2007) is the 3D geometry which takes into account the free surface.

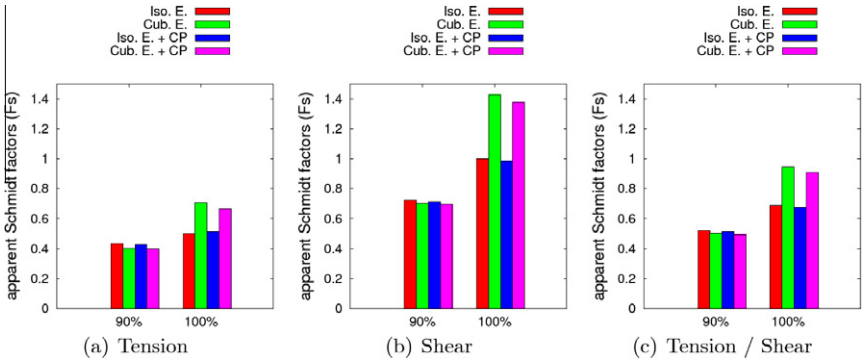

Fig. 19. Apparent Schmidt factors as a function of the percentile. (Cub. E. = cubic elasticity, Iso. E. = isotropic elasticity, CP = crystal plasticity.)

It can be concluded that the grain geometry as well as the influence of neighbouring grains have a large effect on the maximum values of the resolved shear stress in the grains. It can be noted that the grain shape also effects the mesoscopic results.

6. Conclusion

In this work high cycle fatigue behaviour is investigated via the numerical simulation of polycrystalline aggregates. The effects of cubic elasticity and crystal plasticity are clearly distinguished. It is seen that crystal plasticity has a relatively small effect, for the applied load levels (i.e., close to the macroscopic yield stress), but variations exist which are certainly not negligible when dealing with extreme value statistics. Cubic elasticity has a drastic effect on the dispersion of mechanical quantities commonly used in high cycle multiaxial fatigue criteria. The analysis of the Crossland criterion at the mesoscopic scale has shown that the macroscopic criterion prediction is approximately equal to the "average" mesoscopic prediction. The investigation of the two criteria that use a critical plane approach (i.e., Dang Van and Matake) have highlighted the importance of the mesoscopic dispersion for the maximum values of these criteria. Cubic elasticity has a non-negligible effect on the values of the hydrostatic stress and the normal stress. The use of elastic anisotropy at the mesoscopic scale in homogenisation models could improve the predictions of this type of approach. An investigation of the apparent Schmidt factors has shown that the maximum shear stress is much greater for material behaviour including cubic elasticity. However, the same trends can be found with results from the literature by taking the 90th percentile (i.e., the maximum shear stress is lower for cubic elasticity than for isotropic elasticity as discused by Sauzay (2007)).

The perspectives for this work include the analyse of the effect of the critical grain using statistics of extremes (Saintier et al., 2011). Also, using 2D computations allow to have a first picture of the mesoscale response of the microstructure to cyclic loading in fatigue contexte. Full 3D semi-periodic computation dedicated to the free surface effect will form the object of future work.

References

Agbessi, K., Saintier, N., Palin-Luc, T., 2011. Activated slip systems in copper polycrystal under multiaxial fatigue loadings. Advances in Heterogeneous Material Mechanics, 3rd Conference for Heterogeneous Materials Mechanics (ICHMM), Shanghaï

Altus, E., 2006. Microstress estimate of stochastically heterogeneous structures by the functional perturbation method: A one dimensional example. Probabilistic Engineering Mechanics 21 (4), 434–441.

Aubert, I., Saintier, N., Olive, J.-M., 2012. Crystal plasticity computation and atomic force microscopy analysis of the internal hydrogen-induced slip localisation on polycrystalline stainless steel. Scripta Materialia 66 (9), 698–701.

Barbe, F., Quey, R., 2011. A numerical modelling of 3d polycrystal-to-polycrystal diffusive phase transformations involving crystal plasticity. International Journal of Plasticity 27 (6), 823–840.

Bennett, V., McDowell, D., 2003. Polycrystal orientation distribution effects on microslip in high cycle fatigue. International Journal of Fatigue 25 (1), 27–39.

Bertolino, G., Constantinescu, A., Ferjani, M., Treiber, P., 2007. A multiscale approach of fatigue and shakedown for notched structures. Theoretical and Applied Fracture Mechanics 48 (2), 140–151.

Bhandari, Y., Sarkar, S., Groeber, M., Uchic, M., Dimiduk, D., Ghosh, S., 2007. 3d polycrystalline microstructure reconstruction from fib generated serial sections for fe analysis. Computational Materials Science 41 (2), 222–235.

Bridier, F., McDowell, D.L., Villechaise, P., Mendez, J., 2009. Crystal plasticity modeling of slip activity in ti-6al-4v under high cycle fatigue loading. International Journal of Plasticity 25 (6), 1066–1082.

Crossland, B., 1956. Effect of large hydrostatic pressures on the torsional fatigue strength of an alloy steel. Institution of Mechanical Engineers, International Conference on Fatigue on Metals, London, pp. 138–149.

Dang Van, K., 1973. Sur la résistance à la fatigue des métaux. Sciences et Techniques de l'armement, mémorial de l'artillerie française, 3eme facicule.

Fatemi, A., Socie, D.F., 1988. Critical plane approach to multiaxial fatigue damage including out-of-phase loading. Fatigue & Fracture of Engineering Materials & Structures 11 (3), 149–165.

Fernand, Meyer, 1994. Topographic distance and watershed lines. Signal Processing 38 (1), 113–125.

Flaceliere, L., Morel, F., Dragon, A., 2007. Competition between mesoplasticity and damage under hcf – elasticity/damage shakedown concept. International Journal of Fatigue 29 (12), 2281–2297.

Fritzen, F., Böhlke, T., Schnack, E., 2009. Periodic three-dimensional mesh generation for crystalline aggregates based on voronoi tessellations. Computational Mechanics 43, 701–713.

Gérard, C., N'Guyen, F., Osipov, N., Cailletaud, G., Bornert, M., Caldemaison, D., 2009. Comparison of experimental results and finite element simulation of strain localization scheme under cyclic loading. Computational Materials Science 46 (3), 755–760, proceedings of the 18th International Workshop on Computational Mechanics of Materials - IWCMM-1.

Geuzaine, C., Remacle, J.-F., 2009. Gmsh: a three-dimensional finite element mesh generator with built-in pre- and post-processing

facilities. International Journal for Numerical Methods in Engineering 79 (11), 1309–1331.
Groeber, M., Ghosh, S., Uchic, M.D., Dimiduk, D.M., 2008. A framework for automated analysis and simulation of 3d polycrystalline microstructures. Part 2: synthetic structure generation. Acta Materialia 56 (6), 1274–1287.
Guilhem, Y., Basseville, S., Curtit, F., Stéphan, J.-M., Cailletaud, G., 2010. Investigation of the effect of grain clusters on fatigue crack initiation in polycrystals. International Journal of Fatigue 32 (11), 1748–1763.
Lin, T.H., 1957. Analysis of elastic and plastic strains of a fcc crystal. Journal of the Mechanics and Physics of Solids 5, 143.
Lukás, P., Kunz, L., 1989. Effect of mean stress on cyclic stress–strain response and high cycle fatigue life. International Journal of Fatigue 11 (1), 55–58.
Luther, T., Könke, C., 2009. Polycrystal models for the analysis of intergranular crack growth in metallic materials. Engineering Fracture Mechanics 76 (15), 2332–2343.
Matake, T., 1977. An explanation on fatigue limit under combined stress. Bulletin of the JSME 141, 257–263.
Meric, L., Cailletaud, G., 1991. Single crystal modeling for structural calculations: Part 2—finite element implementation. Journal of Engineering Materials and Technology 113 (1), 171–182.
Monchiet, V., Charkaluk, E., Kondo, D., 2006. Plasticity-damage based micromechanical modelling in high cycle fatigue. Comptes Rendus Mécanique 334 (2), 129–136.
Monchiet, V., Charkaluk, E., Kondo, D., 2008. A micromechanical explanation of the mean stress effect in high cycle fatigue. Mechanics Research Communications 35 (6), 383–391.
Morel, F., Huyen, N., 2008. Plasticity and damage heterogeneity in fatigue. Theoretical and Applied Fracture Mechanics 49 (1), 98–127.
Musienko, A., Tatschl, A., Schmidegg, K., Kolednik, O., Pippan, R., Cailletaud, G., 2007. Three-dimensional finite element simulation of a polycrystalline copper specimen. Acta Materialia 55 (12), 4121–4136.
Poncelet, M., Doudard, C., Calloch, S., Weber, B., Hild, F., 2010. Probabilistic multiscale models and measurements of self-heating under multiaxial high cycle fatigue. Journal of the Mechanics and Physics of Solids 58 (4), 578–593.
Przybyla, C.P., McDowell, D.L., 2010. Microstructure-sensitive extreme value probabilities for high cycle fatigue of ni-base superalloy in100. International Journal of Plasticity 26 (3), 372–394.
Saintier, N., Robert, C., Hor, A., Morel, F., Palin-Luc, T., 2011. High cycle fatigue strength criteria and microstructurally related modeling of metals. Advances in Heterogeneous Material Mechanics, In: 3rd Conference for Heterogeneous Materials Mechanics (ICHMM), Shanghaï.
Sauzay, M., 2007. Cubic elasticity and stress distribution at the free surface of polycrystals. Acta Materialia 55 (4), 1193–1202.
St-Pierre, L., Héripré, E., Dexet, M., Crépin, J., Bertolino, G., Bilger, N., 2008. 3D simulations of microstructure and comparison with experimental microstructure coming from o.i.m. analysis. International Journal of Plasticity 24 (9), 1516–1532.
Taylor, G.I., 1938. Plastic strains in metals. Journal Institute of Metals 62, 307.
Weibull, W., 1939. A statistical theory of the strength of materials. Proceedings of the Royal Swedish Institute for Engineering Research, Report, 151.
Weibull, W., 1951. A statistical distribution function of wide applicability. ASME – Journal of Applied Mechanics 18, 293–297.
Weyer, S., Fröhlich, A., Riesch-Oppermann, H., Cizelj, L., Kovac, M., 2002. Automatic finite element meshing of planar voronoi tessellations. Engineering Fracture Mechanics 69 (8), 945–958.
Zhang, K.S., Wu, M.S., Feng, R., 2005. Simulation of microplasticity-induced deformation in uniaxially strained ceramics by 3-d voronoi polycrystal modeling. International Journal of Plasticity 21 (4), 801–834.